CHAPTER 3

PARAMETRIC STUDY OF THE UNIAXIAL TENSION TEST

3.1. INTRODUCTION

In order to further examine the uniaxial tensile test method based on a notched cylindrical specimen, which was proposed and used in Chapter 2, a parametric study was planned and executed to analyze the effects of different variables on the response.

The parameters studied, which may be expected to influence the σ-*w* response, are the slenderness of the cylinder and the notch depth, and the effect of fiber orientation when cores are used. The aspects to be analyzed in the tensile tests are not only the σ-*w* response but also the mode of failure, the rotation of crack faces and the evolution of toughness measures. Additionally, the response of the cylindrical specimens is compared with that of notched panels under uniaxial tension, three-point bend notched beams and splitting-tension test of a disc. Furthermore, the test results are used to propose a multilinear σ-*w* curve to represent the tensile behavior of the SFRC. The individual test data is presented separately in Annex B.

3.2. MATERIALS AND SPECIMENS

A conventional concrete (denoted as N1), with a characteristic strength of 30 MPa, with 40 kg/m^3 of Dramix® RC 80/60 BN hooked-ended steel fibers was used in the study. The concrete composition is given in Table 3.1 and the properties of the fibers, as specified by the manufacturer Bekaert, are shown in Table 3.2. The fibers were of low carbon steel with circular cross-section and collated with a water-soluble glue.

Table 3.1. Composition of concrete

Components (kg/m^3)	
Cement (Type CEM I 52.5R)	349
Crushed limestone gravel (5-12 mm)	978
Crushed limestone sand (0-5 mm)	873
Water added	205
Fibers	40
Active naphthalene-based superplasticizer dosage (% by weight of cement ratio)	0.25
Water/cement ratio	0.57

Table 3.2. Properties of the fibers

Properties	
Length (mm)	60
Aspect ratio (length/diameter)	80
Tensile strength (MPa)	1000
Min. value of max. deformation (%)	0.8

The concrete was mixed in a 250 liter vertical axis forced action mixer. The mixing sequence was the following: the dry components were mixed for 1 minute; then the water was added and mixed for another minute; then, the superplasticizer was incorporated and mixed for 1.5 more minutes; lastly, the fibers were incorporated and the concrete was

mixed for 2 more minutes. The homogeneity of the mix was observed to be satisfactory. Three batches of concrete, denoted as A, B and C, were mixed for the specimens needed for the experimental study. The slump of the fresh concrete, and the mean compressive strength obtained from three 150×300 mm cylindrical specimens are given in Table 3.3.

Table 3.3. Properties of the mixes

Properties	**Batch A**	**Batch B**	**Batch C**
Slump (cm)	8.5	4.5	8.5
f_c (MPa)	44.6 (at 99 days)	41.9 (at 65 days)	36.7 (at 46 days)

From these batches, cylinders of two different sizes: 150×300 mm and 150×450 mm were cast. The cylinders were compacted by tamping them in three layers. This form of compaction was chosen after an independent study at UPC, where it was seen that table-vibration could lead to significant horizontal fiber orientation, which is unfavorable for the tensile test (see Annex C).

Additionally, prismatic elements of 150×150×600 mm were cast in one layer and table vibrated at 50 Hz. The placing of the concrete followed the procedures recommended in the literature (Saldivar, 1999; RILEM, 2000a). After filling the metal moulds, the top surfaces were leveled and covered with a plastic sheet. After 24 hours, the elements were demolded and placed in a fog room (20 ± 2° C and 98% RH) during 28 days and then stored in laboratory environment until the time of testing.

Other than the cylinders for the compressive strength, specimens for uniaxial tension, bending and splitting-tension test were prepared from these elements using the molded specimens as such, by cutting them to the desired size, or by extracting cores from them. Table 3.4 lists the specimens used in the study of the uniaxial tensile behavior.

Table 3.4. Specimens in the uniaxial tension tests

Test series	Variable	Values	Specimen notation
Molded cylinders of 150 mm diameter and notch depth of 15 mm for studying the effect of slenderness	specimen height	150 mm	N1-C-UTM1-n15-1~5
		300 mm	N1-B-UTM2-n15-1~6
		450 mm	N1-B-UTM3-n15-1~6
Molded cylinders of 150 mm diameter and 150 mm height for studying the effect of notch depth	notch depth	10 mm	N1-C-UTM1-n10-1~6
		15 mm	N1-C-UTM1-n15-1~5
		20 mm	N1-C-UTM1-n20-1~6
Cored cylinders of 93 mm diameter, 100 mm height and notch depth of 9.3 mm for comparing the responses of molded and cored specimens	coring direction	vertical	N1-A-UTCV-1~6
		horizontal	N1-A-UTCH-1~6
Double-edge-notched panels of 150 width, 150 mm height and notch depth of 15 mm for comparing the responses with that of the cylinders	panel thickness	25 mm	N1-A-UTP-t25-1~6
		50 mm	N1-A-UTP-t50-1~6

As seen in the above table, the first series deals with specimens with slenderness (height/diameter ratios) of 1, 2 and 3, where the specimens with a height of 150 mm were cut from standard cylinders of 150×300 mm specimens by cutting away 75 mm from each end. The notch depth was maintained in this series as 15 mm, which is 10% of the specimen diameter. Note that the notch depth is the length of the cut (i.e., measured from the specimen surface to the notch root). The circumferential notch was cut at mid-height with a circular diamond-edged saw. In the second series, different notch depths of 10, 15 and 20 mm are cut in the specimen of 150×150 mm. In the third series, tests were performed on cores extracted from the prisms vertically (i.e., along the casting direction) and horizontally (i.e., perpendicular to the casting direction). The cores were of 93 mm diameter and 100 mm height, and 9.3 mm deep circumferential notches were cut in them.

In order to evaluate the differences between the responses of cylindrical and prismatic specimens, panels were cut from the prisms, with the cut face perpendicular to the longitudinal axis of the prism. The load was applied perpendicular to the casting direction. The height and width were 150 mm, and the thickness was 25 or 50 mm. Two

edge notches of 15 mm (i.e., 10% of the specimen width) were cut at mid-height with a diamond band saw.

The specimen notation used in Table 3.4 and the following tables are in accordance with the designations given below :

N1= Mix notation

A, **B** or **C** = batch

UTM1, 2 or 3 = uniaxial tension test on molded cylinder of diameter equal to 150 mm and a slenderness (height/diameter ratio) of 1, 2 or 3, respectively

UTCV = uniaxial tension test on a cored cylinder of diameter equal to 93 mm and a slenderness of about 1, with the core extracted from a prismatic element in the vertical direction (i.e., along the casting direction)

UTCH = uniaxial tension test on a cored cylinder of diameter equal to 93 mm and a slenderness of about 1, with the core extracted from a prismatic element in the horizontal direction (i.e., perpendicular to the casting direction)

n10 = notch depth of 10 mm

n15 = notch depth of 15 mm

n20 = notch depth of 20 mm

UTP = uniaxial tension test on panel of 150 mm height and width, with two 15 mm deep edge notches

t25 = panel thickness of 25 mm

t50 = panel thickness of 25 mm

3PB = three point bending test on center-notched prism, with a square section of 150×150 mm, a span of 500 mm and notch depth of 25 mm

S = splitting tension of a disc of 150 mm diameter and 100 mm thickness

The last number in the specimen notation denotes the trial. For each type of test, 5 or 6 trials were made.

In addition to the specimens in Table 3.4, the notched beam tests and the splitting tension tests were performed on specimens cast in Batch A and C, respectively. The discs for the splitting test were cut from standard cylinders.

3.3. EXPERIMENTAL DETAILS

For the uniaxial tension tests, the surfaces that had to be glued to the loading platens were either cut or polished and then cleaned with a solvent. After preparing the loading surfaces and cutting the notches, the specimens were fixed to the platens of the testing machine using a fast setting two-component glue (X60-NP Schnellklebstoff, HBM, Germany) while applying a small load during the curing of the adhesive (approximately 15 minutes). All tests were carried out with fixed platens, avoiding the rotation of the loading surfaces during the test.

The tests were performed in an Instron 8500 servo-hydraulic testing system (see Figure 2.1) under closed-loop control. In the case of the molded cylinders, the tests were controlled by means of the average crack mouth opening displacement ($\bar{\delta}$) obtained from three extensometers (of 2.5 mm span and 25 mm gauge length) placed around the specimen at 120º to each other, as in Figure 2.2. Additionally, individual measurements (δ_i) around the circumference were made with three LVDTs (of 5 mm span), placed at 120º to each other between two rings mounted on the specimen (see Figure 2.2). Only the average crack mouth opening displacement, $\bar{\delta}$, was measured in the tests on cores and used as the control variable. For practical reasons, the panel specimens were controlled through the average signal of two extensometers (Figure 3.1). Additionally, the crack opening was measured on both edges of the 50 mm thick panels through two LVDTs located at diagonally opposite corners (Figure 3.1). In the case of 25 mm thick panels, there was not enough space for mounting the LVDTs.

The tests were performed with the following $\bar{\delta}$-rate sequence: 5μm/min up to $\bar{\delta}$ = 50 μm, then 100 μm/min up to $\bar{\delta}$ = 1000 μm and 500μm/min then onwards up to $\bar{\delta}$ = 2000 μm. All readings were recorded through the data acquisition unit of the testing system.

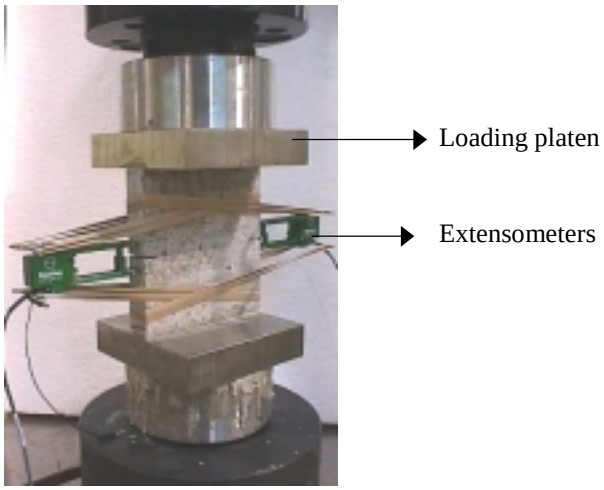

Top view of a 50 mm thick panel

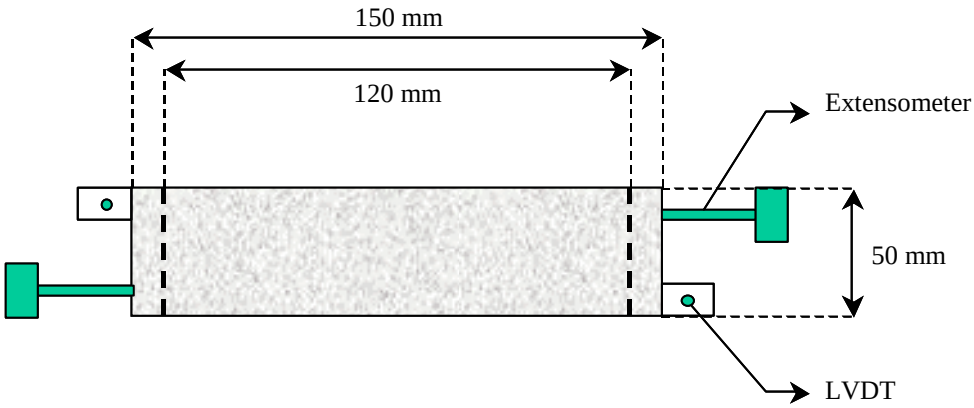

Top view of a 25 mm thick specimen

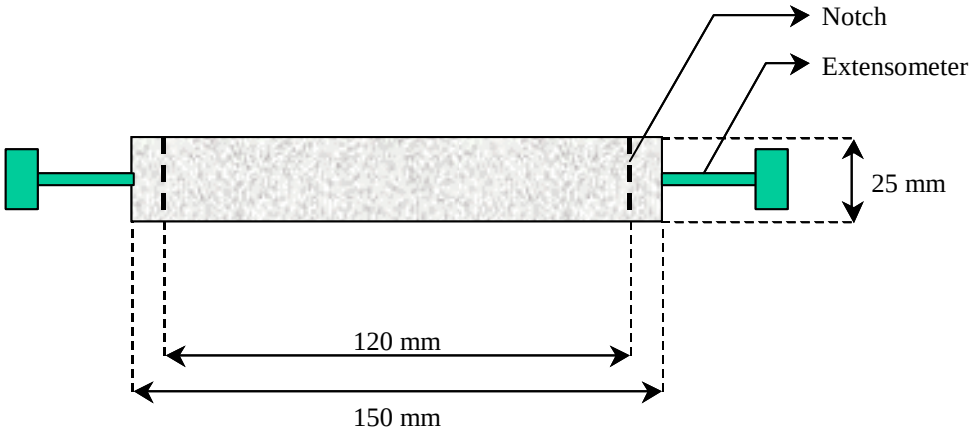

Figure 3.1. Test set-up for prismatic specimens

3.4. PROPERTIES TO BE ANALYZED

3.4.1. σ-w Curve

As mentioned in Chapter 2, the load divided by the net area (or the area of the unnotched ligament) is considered as the applied tensile stress, σ. The crack width, *w*, is calculated, as shown in Figure 3.2, from $\bar{\delta}$ by subtracting the mean displacement at the first peak, $\bar{\delta}_{peak}$ (corresponding to the stress σ_{peak}); i.e., $w = \bar{\delta} - \bar{\delta}_{peak}$, with $w > 0$. The consequent σ-*w* response is given in Figure 3.3.

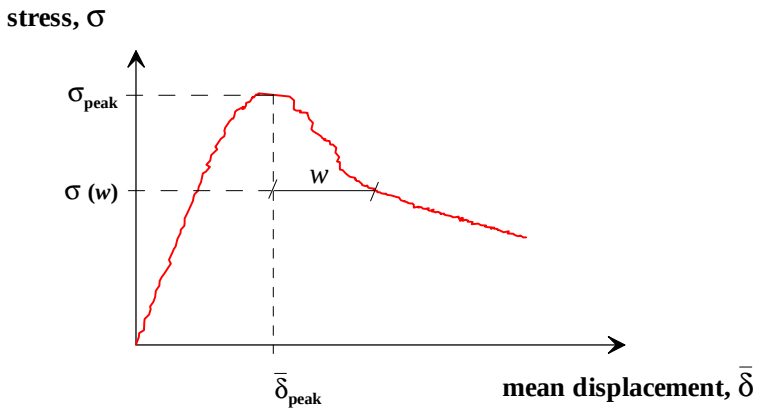

Figure 3.2. Obtaining the σ-*w* relation

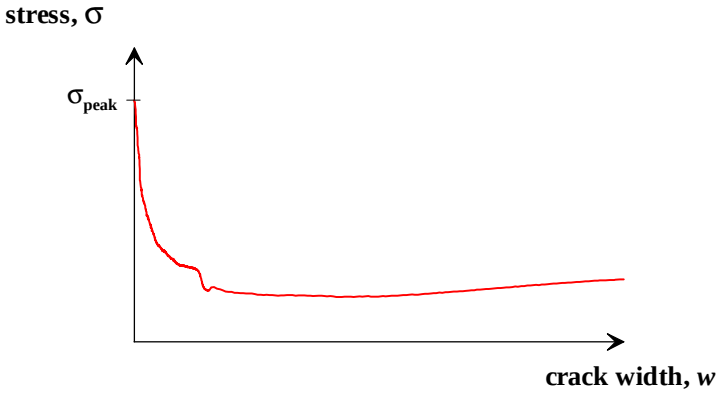

Figure 3.3. σ-*w* relation

3.4.2. Rotation of the Crack Faces

As seen in the previous section, there are significant differences in the individual LVDT readings for small $\bar{\delta}$, which implies considerable rotation of the crack faces with respect to each other. This can be attributed to non-symmetric crack propagation, with the crack starting from one point on the crack tip and propagating over the ligament. This effect can clearly be seen in Figure 3.4, where the individual readings are shown against $\bar{\delta}$.

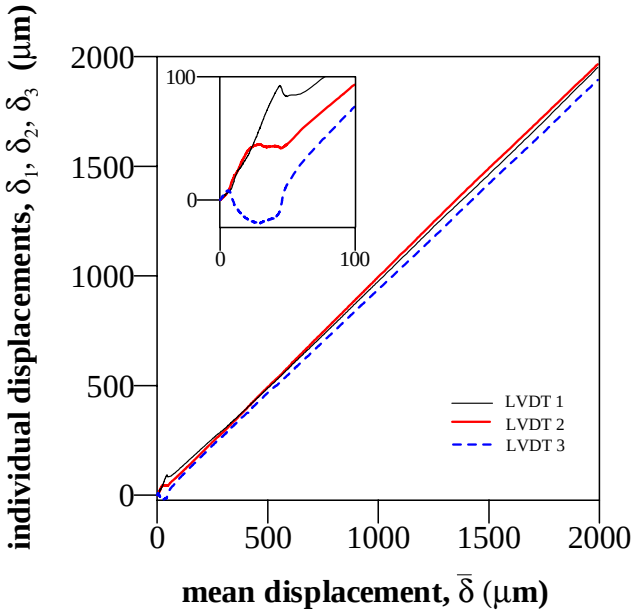

Figure 3.4. Deviation of the individual LVDT readings

In order to quantify the non-symmetry of the crack opening, an angle of relative rotation of the crack faces is calculated from the individual readings (δ_1, δ_2, δ_3). This rotation is given by the angle between the vertical axis and the normal to a plane defined by the readings at any point in time. Considering, the LVDTs positioned at the coordinates (x_i, y_i) with readings δ_i, where i = 1, 2 and 3, the plane is given by:

$$A(x-x_1) + B(y-y_1) + C(z-\delta_1) = 0 \qquad \text{(eq. 3.1)}$$

where

$$A=\begin{vmatrix} y_2-y_1 & \delta_2-\delta_1 \\ y_3-y_1 & \delta_3-\delta_1 \end{vmatrix} \qquad B=\begin{vmatrix} \delta_2-\delta_1 & x_2-x_1 \\ \delta_3-\delta_1 & x_3-x_1 \end{vmatrix} \qquad C=\begin{vmatrix} x_2-x_1 & y_2-y_1 \\ x_3-x_1 & y_3-y_1 \end{vmatrix}$$

The rotation of the plane with respect to the vertical axis of the specimen is then:

$$\alpha = tan^{-1}\left(\frac{\sqrt{A^2+B^2}}{C}\right) \qquad \text{(eq. 3.2)}$$

A typical plot of the evolution of the rotation can be seen in Figure 3.5, which shows the rotations up to a $\bar{\delta}$ = 100 μm on the left and up to $\bar{\delta}$ = 1200 μm on the right.

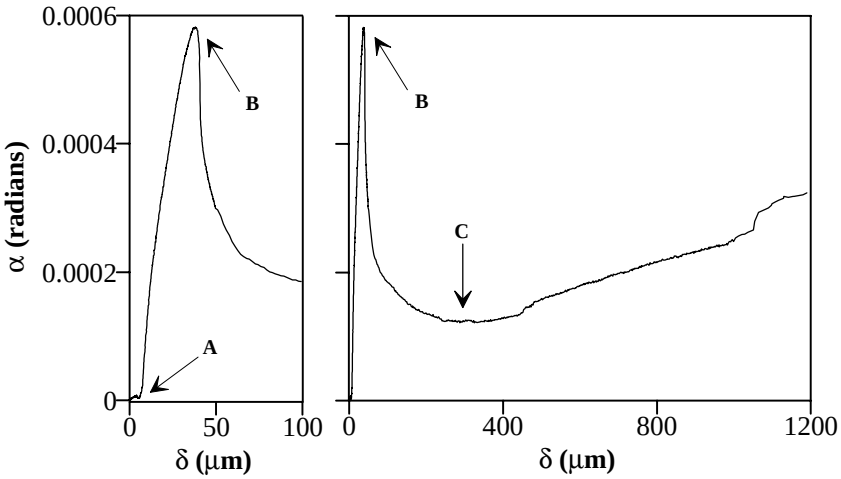

Figure 3.5. Relative rotation of the crack faces during the test

The evolution of the rotation is useful in explaining the failure behavior of the specimen. It can be seen in Figure 3.5. there is some rotation up to peak load (point A in the figure), which can be attributed to non-symmetry of the test setup. More importantly, the rotation increases beyond point A, due to non-symmetric crack initiation and propagation, up to a point where the matrix is completely cracked (i.e., point B). This also coincides with the drop in load seen in the post-peak response in the σ-δ curve. Thereafter,

the crack faces are only bridged by the fibers, which are distributed unevenly in a non-symmetric manner causing some increase in rotation (beyond point C).

3.4.3. Stress and Toughness Parameters

The parameters that will be analyzed are derived from the σ-*w* curve, as shown in Figure 3.6:

σ_{peak} = first-peak stress, which corresponds to the matrix strength

σ_{min} = minimum stress reached after the post-peak drop

w_{min} = crack width corresponding to σ_{min}

σ_{1000} = stress at a crack width of 1000μm.

σ_{2000} = stress at a crack width of 2000μm.

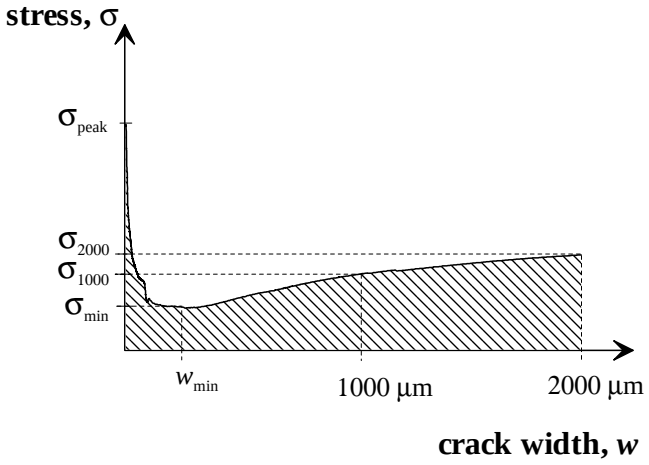

Figure 3.6. Parameters defined in terms of the σ-*w* curve

Regarding the toughness measures, the first parameter that is considered is an absolute measure of toughness, which is directly the area under the σ-*w* curve until a prescribed crack width limit (i.e., the shaded area in Figure 3.6). This is analogous to the fracture energy determined as the area under the complete curve. Using the same notation, the absolute toughness is calculated as:

$$G_F^{w_{lim}} = \int_{w=0}^{w_{lim}} \sigma(w)dw \qquad \text{(eq. 3.3)}$$

where the w_{lim} value defines the point up to which the absolute toughness is evaluated. Two limits have been considered here, w = 1000 μm and w = 2000 μm, which define G_F^{1000} and G_F^{2000}, respectively. Note that the $G_F^{w_{lim}}$-values can be considered as material parameters and are theoretically independent of the geometry or size of the specimen, unlike the toughness obtained from the area under the load-displacement curve of a beam. Also, these values can serve as input parameters in the definition of the constitutive tensile relation of the material in finite element analysis with the cohesive crack or similar model.

Figure 3.7 shows a typical plot of the evolution of $G_F^{w_{lim}}$ with respect to w. The slope of the curve increases up to a w of around 1000 μm, corresponding to the post-peak hardening, and later constant in accordance with the plateau observed in the σ-w curve.

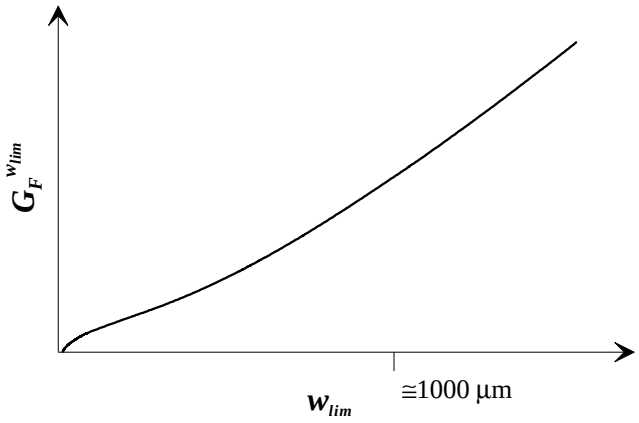

Figure 3.7. Typical evolution of $G_F^{w_{lim}}$ with w

Another toughness parameter that is considered is the *equivalent tensile strength*, denoted as $f_{eq}^{t,w_{lim}}$ and calculated as:

$$f_{eq}^{t,w_{lim}} = \frac{G_F^{w_{lim}}}{w_{lim}} \qquad \text{eq. (3.4)}$$

Note that $f_{eq}^{t,w_{lim}}$ is not the residual strength but an average strength over a range of w (i.e., from $w = 0$ to $w = w_{lim}$). Figure 3.8 shows a typical evolution of $f_{eq}^{t,w_{lim}}$ with w_{lim}. The evolution depends on the residual strengths and the shape is close to that of the σ-w curve.

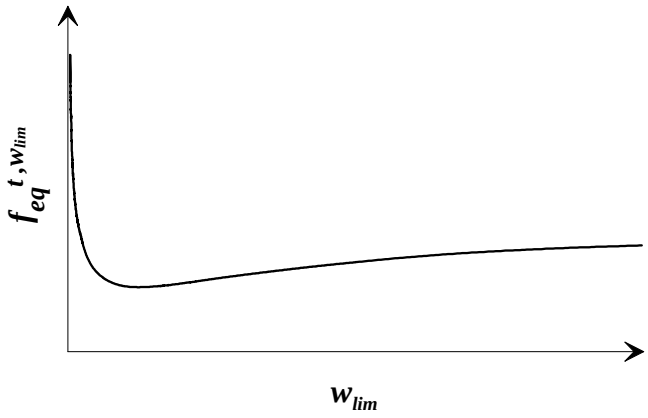

Figure 3.8. Typical $f_{eq}^{t,w_{lim}}$ vs. w_{lim} relation

The values of $f_{eq}^{t,w_{lim}}$ can be used in the drop-constant models of the tensile constitutive stress-crack opening of FRC, where the σ-w curve is modeled by a vertical drop from the tensile strength until the value of $f_{eq}^{t,w_{lim}}$ and a posterior plateau until the $w = w_{lim}$. This approach permits the definition of different post-peak plateaus depending on the maximum crack width to be considered in the analysis.

3.4.4. Total and Effective Fibers

In addition to calculating the stress and toughness based parameters, the fibers crossing the fracture plane have been counted in each case. Since many fibers do not provide crack resistance due to their orientation with respect to the crack, the effective fibers are also counted, where these are the fibers with their hooked ends straightened out indicating their being pulled out.

3.5. RESULTS AND DISCUSSION

In the uniaxial tension test, the failure is expected to occur along the notch plane without significant crack initiation outside the notches. This was the case in all the cylindrical specimens tested here. A photograph of the typical state of the cracked specimen after the test can be seen in Figure 3.9.

Figure 3.9. Fractured cylinder

In the following sections, the mean σ-*w* curves, and the mean values of the calculated parameters and their coefficients of variation are given.

3.5.1. Effects of the Slenderness of the Cylindrical Specimen

Considering the molded cylinders of 150 mm diameter, Figure 3.10 gives the mean σ-*w* behavior for different slenderness ratios. The individual test results are given Annex B (Sections B.1, B.2 and B.3)

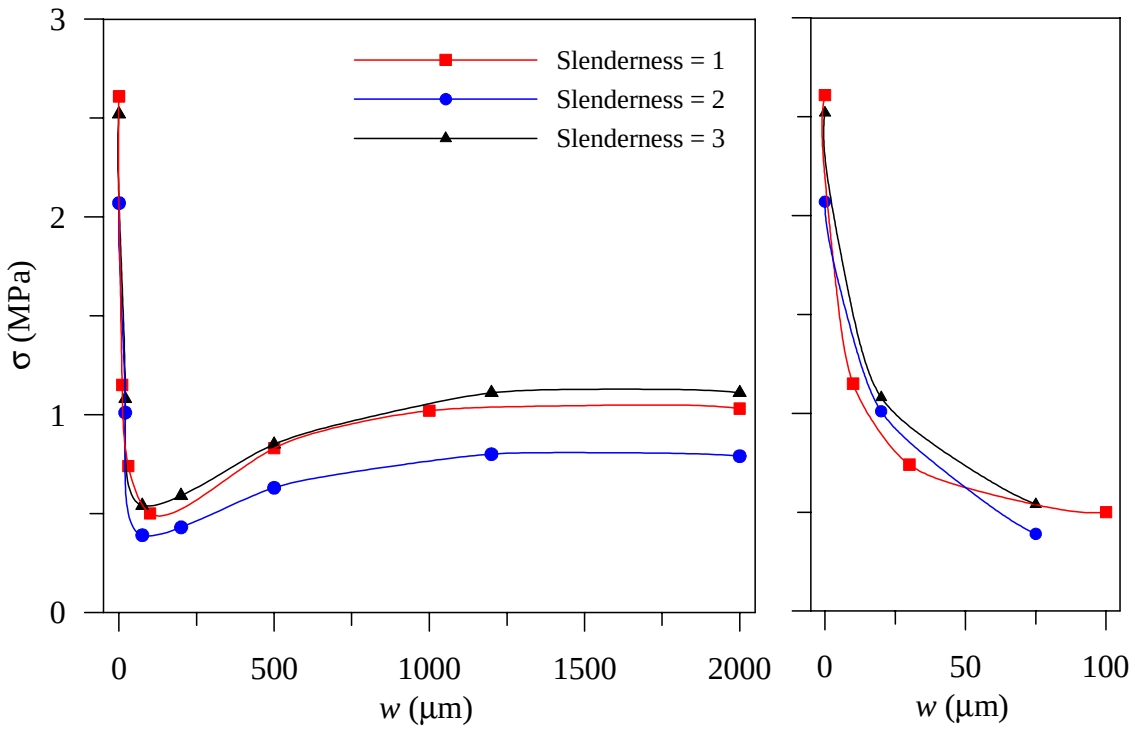

Figure 3.10. σ-*w* responses for specimens of different slenderness

It can be seen that there is no clear tendency in terms of the effect of slenderness (h/Ø) on the response, with very similar behavior in all three cases. The values of the different parameters obtained from the tensile response are given in Table 3.5. Again, no trend can be seen for the effect of slenderness on the mean values of stress and toughness based parameters.

For all post-peak parameters, it seems that variability increases with slenderness, with the parameters corresponding to specimens with h/Ø = 1 generally exhibiting the least scatter. Also, the toughness parameters corresponding to the *w* limit of 1000 μm exhibit less variability than those calculated at 2000 μm.

Table 3.5. Parameters obtained from the specimens of different slenderness ratios

h/Ø	σ_{peak} (MPa)	σ_{min} (MPa)	w_{min} (μm)	α_{peak} (10^{-5} rad)	α_{max} (10^{-3} rad)	σ_{1000} (MPa)	σ_{2000} (MPa)	G_F^{1000} (N/mm)	G_F^{2000} (N/mm)	$f_{eq}^{t,1000}$ (MPa)	$f_{eq}^{t,2000}$ (MPa)	Fibers *Total*	*/Effective*
1	2.6 ± 20%	0.48 ± 15%	99 ± 37%	3.84 ± 75%	1.14 ± 63%	1.0 ± 28%	1.0 ± 30%	0.81 ± 24%	1.84 ± 27%	0.81 ± 23%	0.92 ± 27%	62 ± 17%	34 ± 34%
2	2.1 ± 7%	0.30 ± 16%	94 ± 64%	4.70 ± 22%	0.81 ± 40%	0.7 ± 41%	0.7 ± 38%	0.60 ± 36%	1.34 ± 38%	0.60 ± 35%	0.67 ± 37%	48 ± 14%	25 ± 35%
3	2.5 ± 5%	0.51 ± 30%	126 ± 33%	4.92 ± 42%	0.77 ± 20%	1.1 ± 42%	1.1 ± 44%	0.84 ± 38%	1.96 ± 40%	0.84 ± 38%	0.98 ± 41%	70 ± 36%	41 ± 38%

The values of two rotations are also given in the above table: α_{peak} at the peak load and the maximum rotation during the test α_{max}. A clear effect of the slenderness can be observed in the case of the rotation of the crack faces at peak stress, with α_{peak} increasing with an increase in slenderness, as can be expected due to the decrease in the bending stiffness of the specimen. However, this relative rotation is very small (i.e., less than 5×10^{-5} rad) compared with the maximum rotation α_{max}, which interestingly decreases, though slightly, with an increase in slenderness. The order of magnitude of the maximum rotation seems to be about 1×10^{-3} rad.

Taking into account the lower variability of the post-peak parameters, which are of principal interest here, and the difficulty in handling larger specimens, the slenderness ratio of 1 (i.e., cylinder of 150×150 mm) will be used as the reference in the rest of the study. This corresponds to the test configuration recommended by RILEM (2001).

3.5.2. Effects of the Notch Depth of the Cylindrical Specimen

Figure 3.11 shows the mean σ-w curves for 150×150 mm specimens with notch depths of 10, 15 and 20 mm. It can be observed that, in general, the behavior is very similar, with the 20 mm notch specimens exhibiting higher σ_{peak} and a steeper drop after the peak. Individual test results can be found in Annex B (Figures and Tables B.2, B.4 and B.5).

Table 3.6 gives the parameters for each notch depth. It can be observed that the notch depth influences the peak stress slightly, with higher maximum stress for deeper notches. Also, specimens with a 20 mm notch exhibit almost 35% lower σ_{min}-values with respect to those of 15 mm notch depth. However, there is no significant difference in this respect between the specimens with 10 mm and 15 mm notches. On the other hand, w_{min}-values decrease significantly with an increase in notch depth reflecting the sharper post-peak drop, which can be attributed to a higher stress concentration.

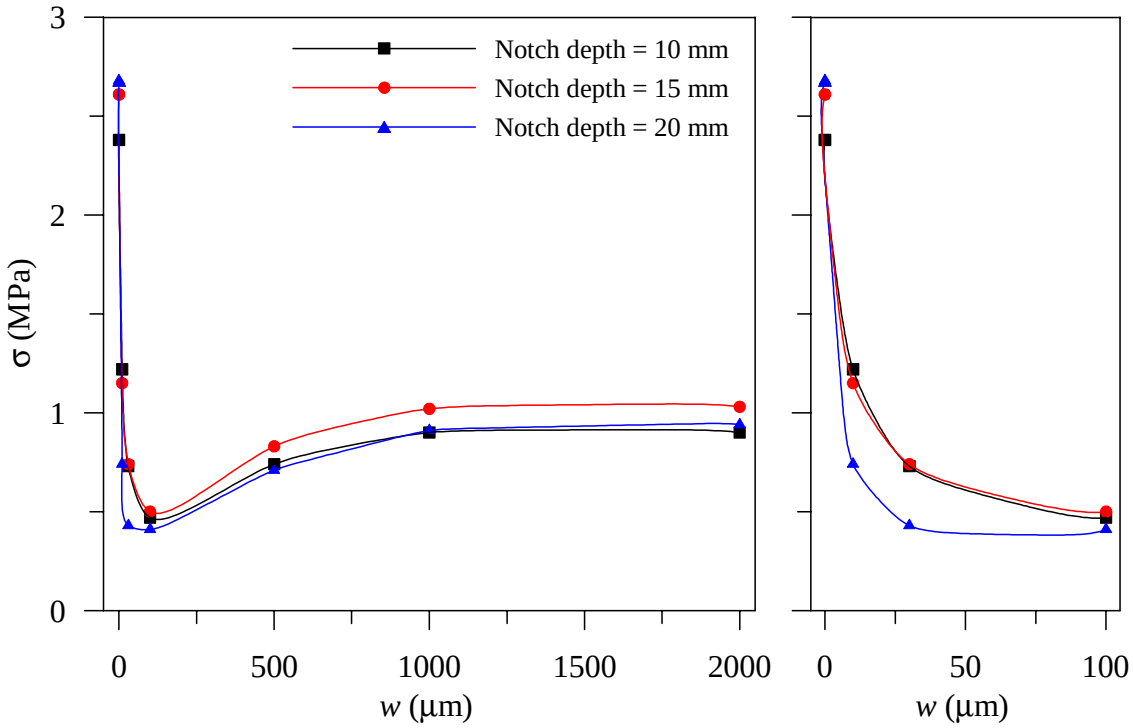

Figure 3.11. σ-*w* responses for specimens with different notch depths

Table 3.6. Parameters obtained specimens with different notch depths

Notch (mm)	σ_{peak} (MPa)	σ_{min} (MPa)	w_{min} (μm)	α_{peak} (10^{-5} rad)	α_{max} (10^{-3} rad)	σ_{1000} (MPa)	σ_{2000} (MPa)	G_F^{1000} (N/mm)	G_F^{2000} (N/mm)	$f_{eq}^{t,1000}$ (MPa)	$f_{eq}^{t,2000}$ (MPa)	**Fibers** *Total/Effective*	
10	2.4 ± 26%	0.45 ± 20%	115 ± 29%	5.87 ± 44%	1.46 ± 18%	0.9 ± 19%	0.9 ± 21%	0.72 ± 18%	1.66 ± 19%	0.72 ± 17%	0.83 ± 18%	58 ± 20%	33 ± 21%
15	2.6 ± 20%	0.48 ± 15%	99 ± 37%	3.84 ± 75%	1.14 ± 63%	1.0 ± 28%	1.0 ± 30%	0.81 ± 24%	1.84 ± 27%	0.81 ± 23%	0.92 ± 27%	62 ± 17%	34 ± 34%
20	2.7 ± 9%	0.36 ± 9%	63 ± 59%	2.98 ± 65%	1.60 ± 37%	0.9 ± 23%	0.9 ± 21%	0.69 ± 20%	1.64 ± 20%	0.69 ± 20%	0.82 ± 20%	45 ± 18%	27 ± 16%

The trends in $G_F^{w_{lim}}$ and, consequently, in the equivalent tensile strengths are practically independent of the notch depth, with slightly higher values for the notch depth of 15 mm. This may be attributed to the wall effect in the case of the specimens with 10 mm notches that would affect the orientation of the fibers near the surface of the specimen and to the reduction of the ligament area in the case of the 20 mm notch that would decrease the number of active fibers. The later effect is seen in the lower number of fibers on the crack surface (i.e., 45 total fibers for the 20 mm notch compared with 62 for a 15 mm deep notch).

The relative rotation of the crack faces at peak stress, α_{peak}, is found to decrease as the notch depth increases. On the other hand, α_{max} is almost constant and in the order of 1-2×10^{-3} rad. This probably implies that the rotation depends basically on the flexural stiffness of the specimen.

Considering the above results and the fact that a shallow notch may lead to the initiation of the crack outside the notch (as seen in Chapter 2), a 15 mm deep notch appears to be the most acceptable for the molded cylinder with a diameter of 150 mm (i.e., the notch depth is 10% of the specimen diameter).

3.5.3. Behavior of Cores

Considering the possibility of the determination of the tensile constitutive relation of the material in existing structures, the behavior of cores was also studied. With this aim, ∅ = 93 mm cores were extracted from 150×150×600 mm prisms, both in the filling (or casting) direction and perpendicular to it, as in Figure 3.12. Since the prisms were compacted by table vibration, it is expected that the fibers will be preferentially oriented along horizontal planes (Saldivar, 1999). Therefore, the response of the core would depend significantly on its original orientation with respect to the casting direction.

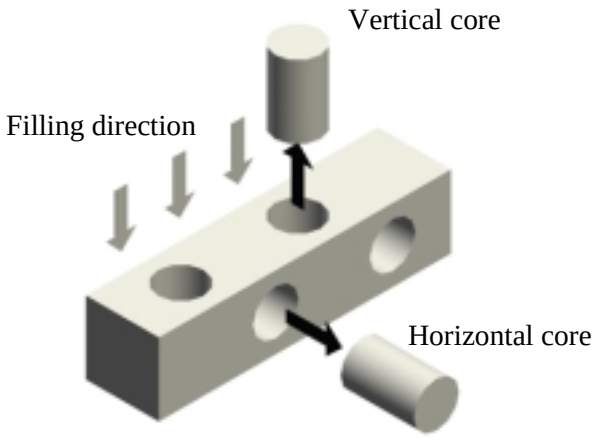

Figure 3.12. Extraction of cores

Figure 3.13 shows the average σ-*w* responses for the case of cores extracted in each direction; the individual data for all the cores can be found in Annex B in Figures and Tables B.6 and B.7. It can be seen that cores obtained vertically (i.e., along the casting direction) yield lower post-peak strengths than those extracted horizontally (i.e., perpendicular to the casting direction).

Along with the mean curves of the cores, the diagram corresponding to the molded 150×150 mm cylinders is plotted as a reference. Note that the slenderness ratio is about one and the notch depth is 10% of the cylinder diameter in all the cases. It can be seen that the response of the molded cylinder lies closer to that of the horizontal cores and exhibits a similar trend with lower residual strengths. This implies that stronger fiber orientation in

the horizontal cores and the absence of wall effects leads to higher toughness than in the molded cylinders.

Considering that the orientation of the fibers in the molded cylinder (compacted by normal tamping) to be practically isotropic, it can be seen that the behavior is a conservative estimate of the behavior of the concrete with fibers oriented preferentially along the direction of loading. On the other hand, the behavior of the vertical cores is much poorer due to the orientation of the fibers mainly along planes parallel to the crack.

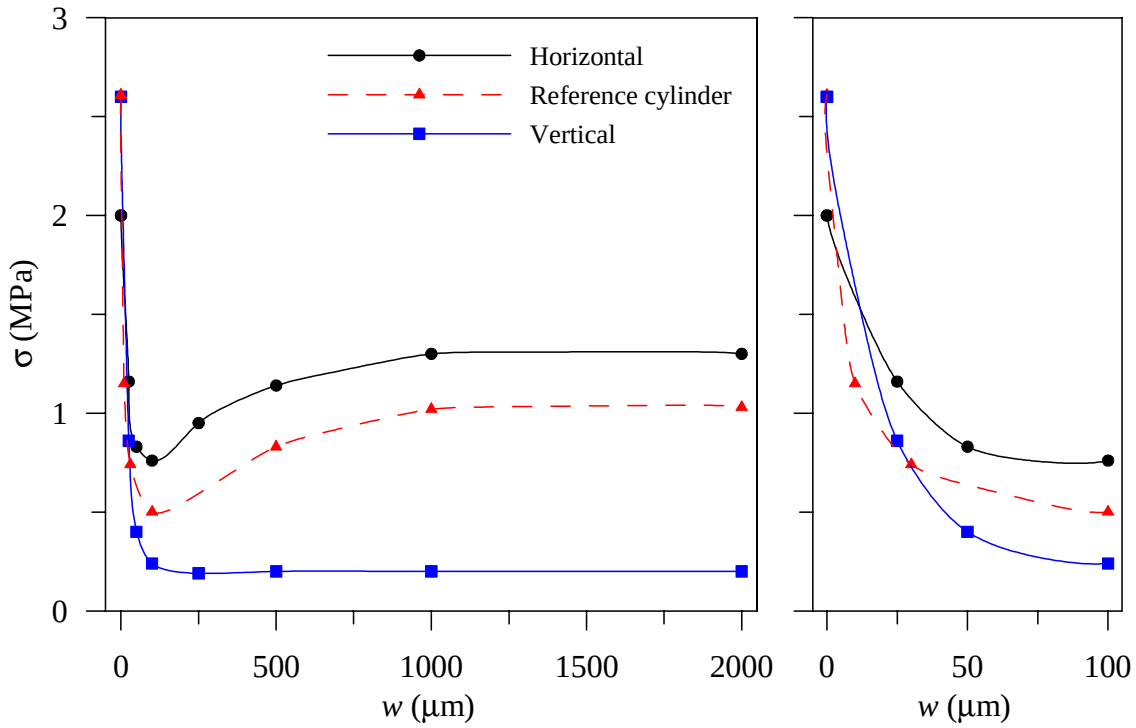

Figure 3.13. σ-*w* responses of cores and molded cylinders

As seen in Table 3.7, the poorer post-peak response of the vertical cores is also reflected in the values of the stress and toughness parameters. The number of fibers seen on the crack faces in each case also shows the preferential orientation of the fibers. The most favorable orientation leads to hardening-type behavior after the post-peak drop and results in the high values of the toughness.

Table 3.7. Mean properties of the cores

Orientation	σ_{peak} (MPa)	σ_{min} (MPa)	w_{min} (μm)	σ_{1000} (MPa)	σ_{2000} (MPa)	G_f^{1000} (N/mm)	G_f^{2000} (N/mm)	$f_{eq}^{t,1000}$ (MPa)	$f_{eq}^{t,2000}$ (MPa)	Fibers *Total /Effective*
Vertical	2.6 ± 9%	0.19 ± 28%	293 ± 40%	0.2 ± 26%	0.2 ± 30%	0.26 ± 23%	0.48 ± 23%	0.26 ± 23%	0.24 ± 24%	18 ± 32% 3 ± 59%
Horizontal	2.0 ± 17%	0.74 ± 18%	90 ± 38%	1.3 ± 24%	1.3 ± 26%	1.11 ± 23%	2.46 ± 23%	1.11 ± 22%	1.23 ± 24%	28 ± 38% 13 ± 54%

From a practical point of view, it is very interesting that the same test method can be used for the characterization of "virgin" material through molded specimens and of the material within an existing structure. It has been shown that this is possible through the uniaxial tensile test configuration, where both molded cylinders and cores can be used. However, the direction of extraction of cores from an existing structure should be taken into account in the interpretation of results from tests on cores. On the other hand, the extraction of cores in several directions would permit the evaluation of the existence of preferentially-oriented fibers due to the compaction process and the effect of this phenomenon on the tensile behavior.

3.5.4. Relation between the Post-Peak Parameters and the Number of Effective Fibers

It can be observed in the tables of the previous sections that the variability in the results is, in general, quite high. Nevertheless, the scatter in the number of fibers across the crack face also varies significantly. In order to examine the dependence of the values of the stress and toughness based parameters obtained from each specimen on the active fibers, six representative parameters (σ_{peak}, σ_{min}, σ_{1000}, σ_{2000}, $f_{eq}^{t,1000}$ and $f_{eq}^{t,2000}$) are plotted in Figures 3.14 to 3.19 with respect to the number of effective fibers, for all the specimens based on molded cylinders. As mentioned earlier, the effective fibers are taken as those with their hooked ends straightened out indicating their being pulled out. Note that the value of R^2 denotes the regression coefficient of the fit.

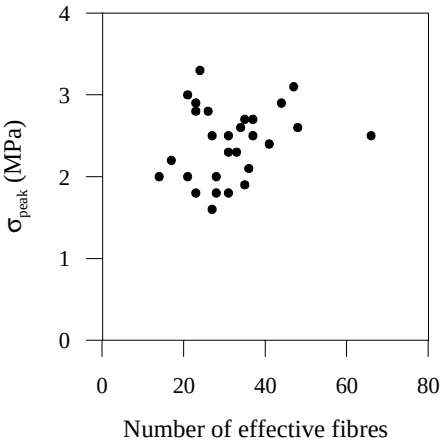

Figure 3.14. σ_{peak} vs. effective fibers

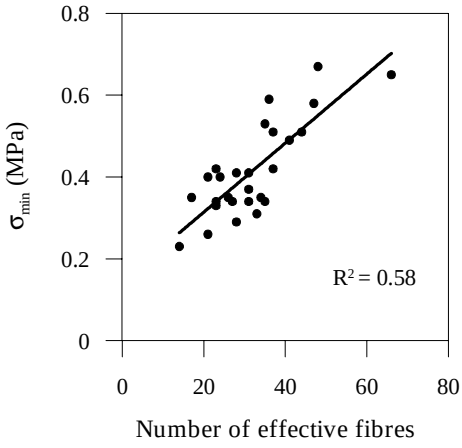

Figure 3.15. σ_{min} vs. effective fibers

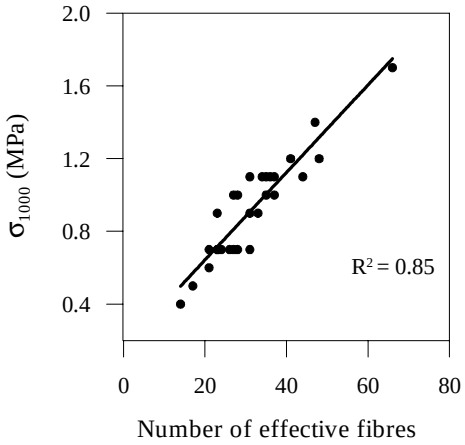

Figure 3.16. σ_{1000} vs. effective fibers

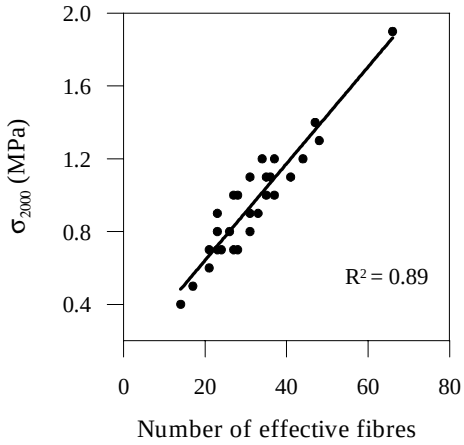

Figure 3.17. σ_{2000} vs. effective fibers

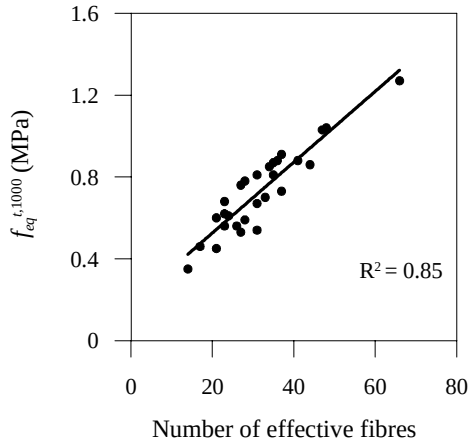

Figure 3.18. $f_{eq}^{t,1000}$ vs. effective fibers

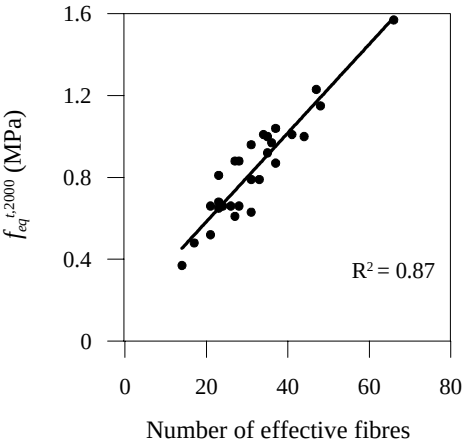

Figure 3.19. $f_{eq}^{t,2000}$ vs. effective fibers

It can be seen in the above figures that the post-peak parameters are significantly dependent on the effective fiber count. In Figure 3.14, no trend can be identified between the maximum stress and the number of effective fibers confirming that this parameter is dominated basically by the matrix behavior. In the case of σ_{min} (see Figure 3.15), there is some dependence on the fiber count indicating the combined influence of the matrix and the fibers on the behavior at this stage. More importantly, there is a linear dependence of the post-peak parameters on the fibers bridging the crack, as seen in Figures 3.16-3.19. This correlation, first of all, points out the cause of the variability in the toughness results and suggests that the use of a larger number of specimens would decrease the variations in the parameters. Secondly, this trend implies that the parameters could be associated with the fiber count or the density of fibers, leading to more reliable material parameters.

3.5.5. Results of Tests on Panels

Edge-notched panels have been used for the determination of the tensile stress-crack opening relation by several researchers (see review in Chapter 1). In order to compare the response of the cylinders with such panels, square slices with heights and widths of 150 mm (similar to the corresponding dimensions of the reference specimen) were cut from the 150×150×600 mm prisms. Panels with two different thicknesses, 25 and 50 mm, were tested. Two edge notches of 15 mm depth (same as the depth of the reference notch in the reference specimen) were cut at mid-height. The test configuration can be seen in Figure 3.1. The tensile load was applied after gluing the panel to fixed loading platens and the direction of loading was perpendicular to the casting direction. The typical mode of failure of the 50 mm thick panels can be seen in Figure 3.20. In the thinner panels, the cracks sometimes deviated significantly from the notch plane (e.g., Figure 3.21), leading to loss of control in the test.

Figure 3.20. Failure plane of the 50 mm thick panel

Figure 3.21. Example of unexpected failure in some 25 mm thick panels

In the case of the 50 mm thick panels, as seen in Figure 3.1, an LVDT was placed on either edge of the specimen to monitor the differential crack opening across the width. Figure 3.22 shows that there are significant differences between the individual LVDT readings for small crack openings, even more than in the case of cylinders. The trends of the curves indicate that while the crack initiates from the edge where LVDT 1 is located and the corresponding notch mouth opens, the other notch closes.

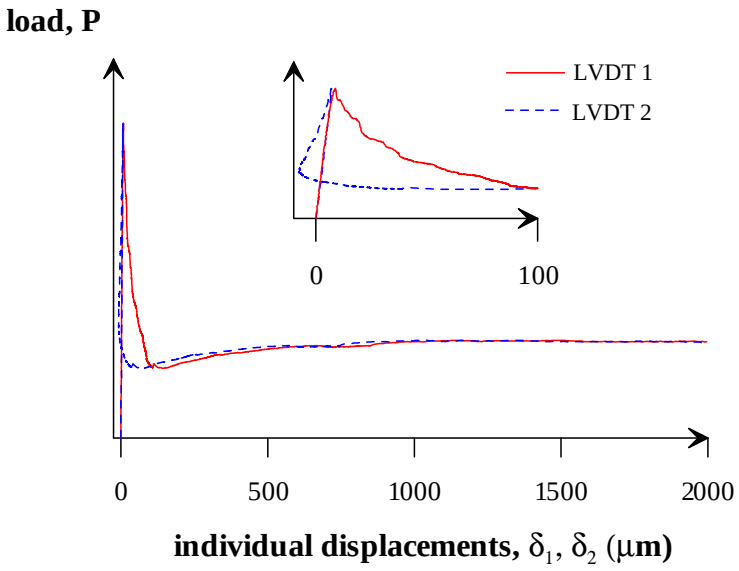

Figure 3.22. Typical load-δ_i response obtained from two LVDTs

The non-symmetric crack opening is clearer in Figure 3.23, where the two LVDT readings are plotted with respect to the average value.

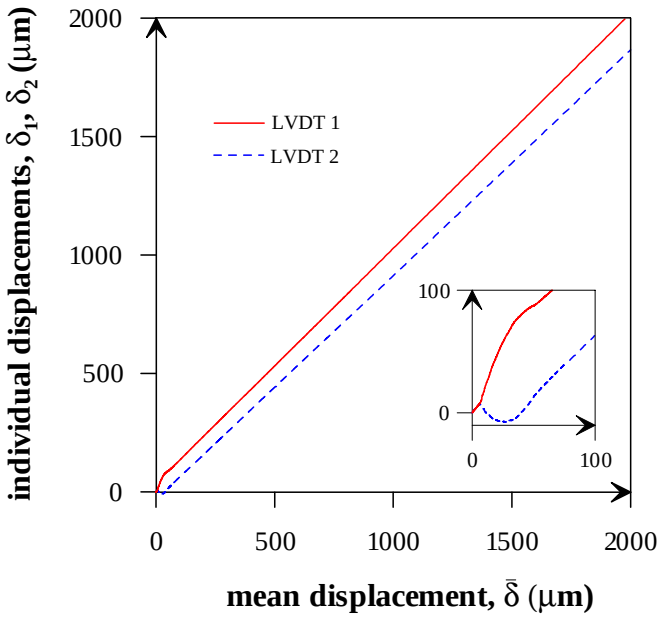

Figure 3.23. Deviation of the individual LVDT readings

The variation of the crack opening across the thickness is not significant, as indicated by the plots in Figure 3.24, where the average value from the two LVDTs is compared with the average obtained from the extensometers located at the opposite ends of the notches. It is seen that the average obtained from both pairs of transducers gives the same values for $\bar{\delta}$.

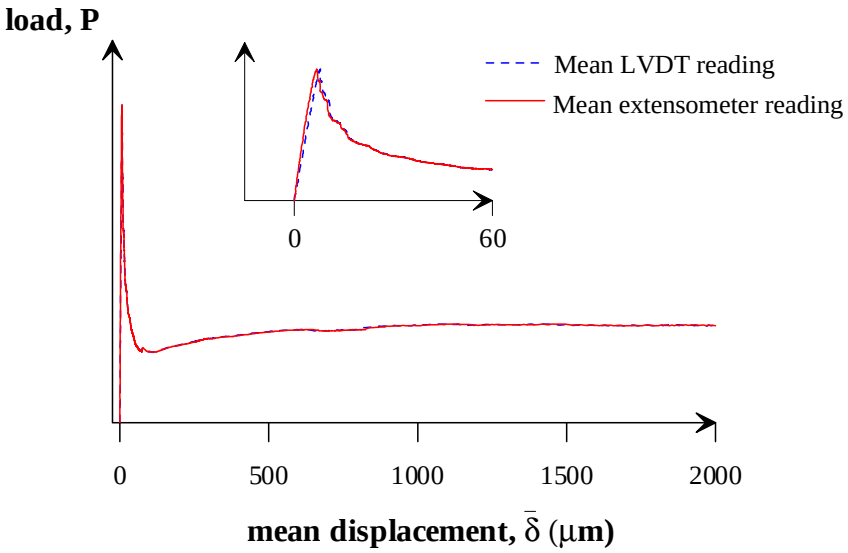

Figure 3.24. Load versus mean crack opening ($\bar{\delta}$) response

In order to quantify the relative rotation of the crack faces, the angle of rotation is calculated from the individual readings of the LVDTs (δ_1 and δ_2). This gives the inclination of the diagonal across the cross section plane. A typical plot of the evolution of the rotation can be seen in Figure 3.25, which shows the rotations up to $\bar{\delta}$ = 70 μm on the left and up to $\bar{\delta}$ = 1000 μm on the right. As it can be seen, the trend of the rotational behavior of the panels is similar to that of the cylinders (section 3.4.2). However, rotations (α_{peak} and α_{max}) are much smaller in the case of panels.

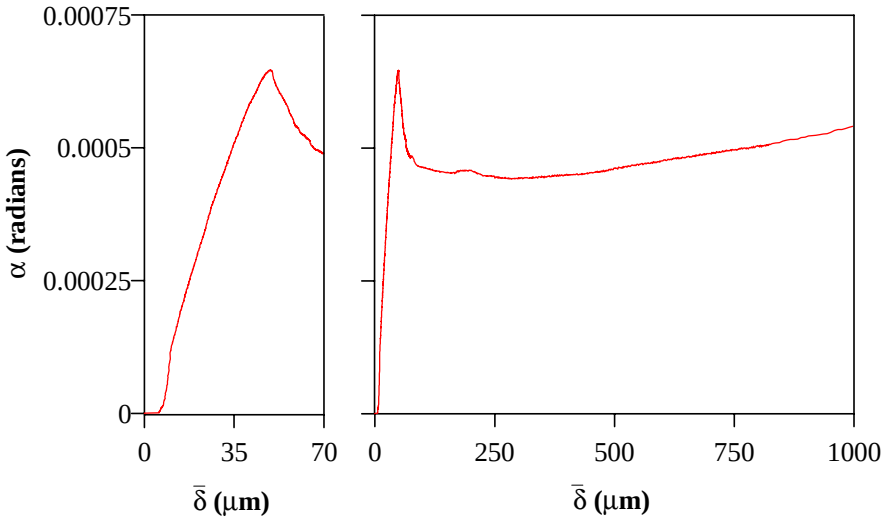

Figure 3.25. Relative rotation of the panel crack faces during the test

Figure 3.26 shows the average σ-*w* plots for the panels, where it can be observed that the forms of the curves are similar with the 25 mm thick panels giving lower residual strengths than the 50 mm thick panels. There is a sharp post-peak drop in both cases followed by some hardening in the 50 mm thick specimens. This difference can be attributed to the fact that the thickness of 25 mm is much smaller than the length of the fiber (i.e., 60 mm), which results in few effective fibers. Individual test results of the panels can be found in Annex B (Figures and Tables B.8 and B.9).

The results from the panels are also compared with the mean response of the reference cylindrical specimen. It can be seen that both panels exhibit lower residual strengths than the cylinder. This is due to the much smaller ligament area and the cutting of several fibers due to the small thickness. The testing of thicker specimens (e.g., 100 mm) was attempted but was not successful due to the failure of the bond at the loading surfaces before fracture. Also, the use of thicker specimens results in uneven through-thickness cracking, which is a problem for the measurement of the crack opening and for the test control.

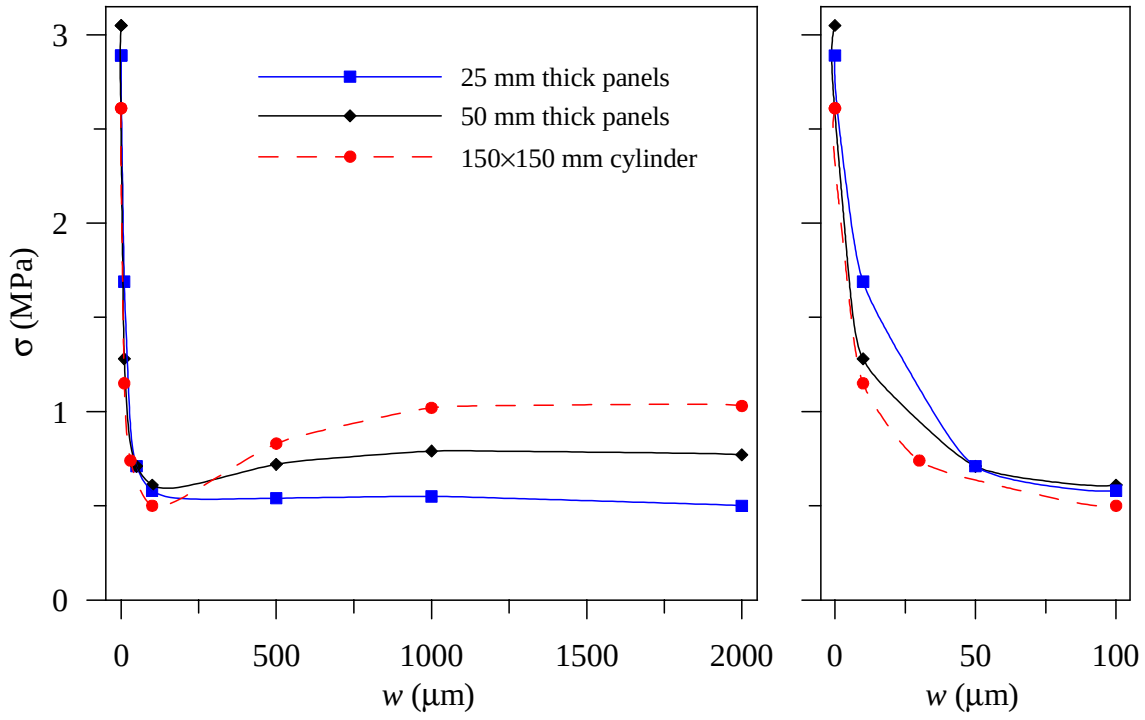

Figure 3.26. σ-*w* responses for panels of different widths

Table 3.8 shows the values of the toughness parameters, indicating higher values for the 50 mm panels with lower variability (i.e., almost the same as in the reference cylinders). As mentioned already, the smaller thickness results in few effective fibers making the test non-representative for the material.

Table 3.8. Mean values of the parameters obtained from the panels

Width (mm)	σ_{peak} (MPa)	σ_{min} (MPa)	w_{min} (μm)	α_{peak} (rad $^{-5}$)	α_{max} (rad $^{-3}$)	σ_{1000} (MPa)	σ_{2000} (MPa)	G_f^{1000} (N-mm)	G_f^{2000} (N-mm)	$f_{eq}^{t,1000}$ (MPa)	$f_{eq}^{t,2000}$ (MPa)	**Fibers** *Total*	*/Effective*
25	2.7 ± 23%	0.47 ± 54%	124 ± 42%	N.M.	N.M.	0.6 ± 61%	0.5 ± 61%	0.59 ± 41%	1.12 ± 48%	0.59 ± 40%	0.56 ± 47%	17 ± 29%	3 ± 74%
50	3.1 ± 10%	0.59 ± 23%	138 ± 30%	1.24 ± 90%	0.69 ± 31%	0.8 ± 28%	0.8 ± 29%	0.73 ± 23%	1.52 ± 25%	0.73 ± 24%	0.76 ± 27%	35 ± 36%	10 ± 41%

N.M. – not measured

Considering the panel specimen results, it is clear that the cylinders yield more representative material behavior than the panels. Therefore, the use of thin panels is not recommended for characterizing the behavior of concrete reinforced with fibers that are longer than the thickness of the panels.

3.6. REPRESENTATIVE σ-*w* CURVE

Considering the response obtained in the test of a molded 150×150 mm cylinder, with a 15 mm notch, as the reference material property, a representative curve defined by 4 points can be proposed for use in finite element or similar analysis. The proposed trilinear curve is presented in Figure 3.27, and is defined by four stresses: peak stress (σ_{peak}), minimum stress (σ_{min}), σ_{1000} and σ_{2000}, in addition to the crack width corresponding to the minimum stress (w_{min}). Considering the results obtained from the 80 uniaxial tension tests carried out for this parametric study and other data (a total of approximately 300 tests), a conservative value for w_{min} would be 20 μm. Nevertheless, this can be identified from the test results as done in the previous section of the report.

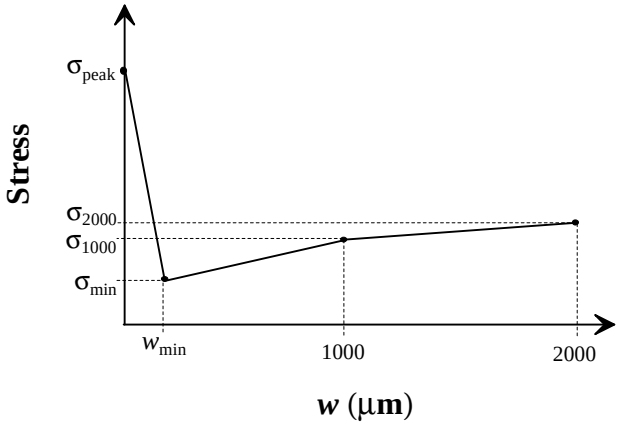

Figure 3.27. Trilinear form of the idealized σ-*w* curve

3.7. FLEXURAL TESTS

In order to provide a more complete set of data, companion flexural tests were performed on notched beams. The configuration given in the RILEM Recommendation (2000a) was also employed here. This is in line with the notched beam tests under center-point loading or three-point bending performed previously by other researchers (Jenq and Shah, 1986; Jamet et al., 1995; Barr et al., 1996; Saldivar, 1999).

The test is performed on a 150×150×600 mm notched prism, with a 500 mm span, subjected to three-point bending, as in Figure 3.28. The test was controlled by means of CMOD (using a clip-on extensometer with a ±2.5 mm span and 10 mm gauge length) and the deflection was also measured using a yoke mounted on the specimen.

Figure 3.28. Flexure test set-up

Typical load-CMOD and load-deflection curves are shown in Figures 3.29a and 3.29b, respectively. The response exhibits significant post-peak hardening, which was not seen in the tension tests. Individual test results can be found in Annex B (Figures and Tables B.10 and B.11).

Table 3.9 summarizes the mean values of the parameters calculated from the flexure test. The limit of proportionality, $f_{ct,fl}$, is obtained as:

$$f_{ct,fl} = \frac{3.F_u.L}{2.b.h_{sp}^2} \qquad \text{(eq. 3.5)}$$

where F_u = load at the limit of proportionality

L = span of the specimen

b = width of the specimen

h_{sp} = net height or ligament depth

The deflection at the limit of proportionality has been denoted as δ_{FU} and the deflection at the minimum load after the post-peak drop as δ_{min}. Considering the equation used for $f_{ct,fl}$, along with the minimum load, we obtain a minimum equivalent stress $f_{ct,fl}^{min}$.

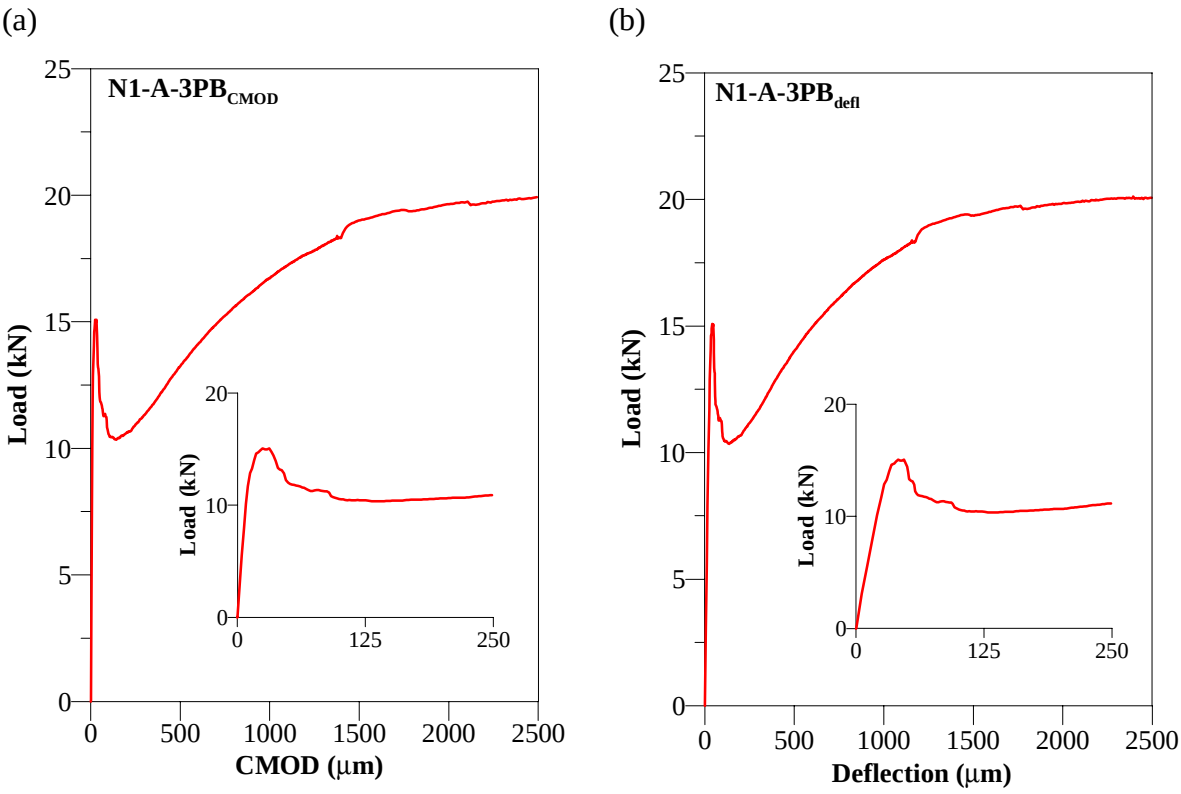

Figure 3.29. Typical (a) load-CMOD and (b) load-deflection curves from the notched beam test

Table 3.9. Flexural test results

Response	$f_{ct,fl}$ (MPa)	$f_{ct,fl}^{min}$ (MPa)	δ_{Fu} (μm)	δ_{min} (μm)	$f_{eq,2}$ (MPa)	$f_{eq,3}$ (MPa)	Number of fibers Total / Effective
Load-deflection	4.45	3.34	45	126	3.39	4.89	140 / 102
Load-CMOD			22	106	3.36	-	

The parameters $f_{eq,2}$ and $f_{eq,3}$ are the equivalent flexural strengths as in RILEM (2000a), when calculated from the load-deflection response. When the load-CMOD response is used, the area under the curve is taken until the CMOD limit that is equal to a corrected deflection limit, where the correction factor is 0.86 (as obtained by a linear fit of the relation between deflection and CMOD). Note that the value of $f_{eq,3}$ could not be calculated since the limit of the CMOD gage was reached before the end of the test.

Additionally, in order to compare the flexural response with that obtained under uniaxial tension, representative peak and post-peak strengths are given in Table 3.10. The values given for the uniaxial tension correspond to the reference 150×150 mm molded cylinder with a 15 mm notch.

Table 3.10. Comparison of the flexural and uniaxial tension test results

Loading	**Tensile strength** (MPa)	**Residual/ Equivalent strengths** (MPa)	
Uniaxial tension	$\sigma_{peak} = 2.6$	$\sigma_{1000} = 1.0$	$\sigma_{2000} = 1.0$
Flexure: load-deflection	$f_{ct,fl} = 4.5$	$f_{eq,2} = 3.39$	$f_{eq,3} = 4.89$

It can be seen that in the comparison of the uniaxial tension and flexural behavior, the peak values are significantly different, with the uniaxial tensile strength being about 60% of the value obtained in flexure. This in accordance with the design equations in Eurocode 2 (1992). In the post-peak regime, the uniaxial tensile residual strength is much more lower than the equivalent flexural strengths. This is because the tensile response exhibits a plateau after a significant post-peak drop while there is some hardening-type behavior after a smaller post-peak drop in the flexural response.

An inverse analysis of the notched beam tests of the previous section has been carried out to obtain the σ-*w* response. The method developed by Professor Jose Luis Antunes de Oliveira e Sousa has been used to obtain the numerical tensile response; a detailed description is given in Annex D. The load-CMOD curve from the beam test is used to obtain the best fitting σ-*w* curve through an optimization technique.

In Figure 3.30, the σ-*w* curves obtained from the inverse analysis of the three beams are compared with the experimentally obtained response from 150×150 mm molded cylinders and cores extracted perpendicular to the casting direction. As it can be seen, there is considerable scatter in the curves from the inverse analysis of the beams. However, it is clear that they are closer to the experimental results from cored specimens with the molded

specimens giving much lower stresses. This can be explained by considering that there is a same preferential alignment of the fibers with respect to the applied stress in the case of beams and cores. On the other hand, a more isotropic distribution is expected in the case of molded cylinders and this is reflected in the obtained response.

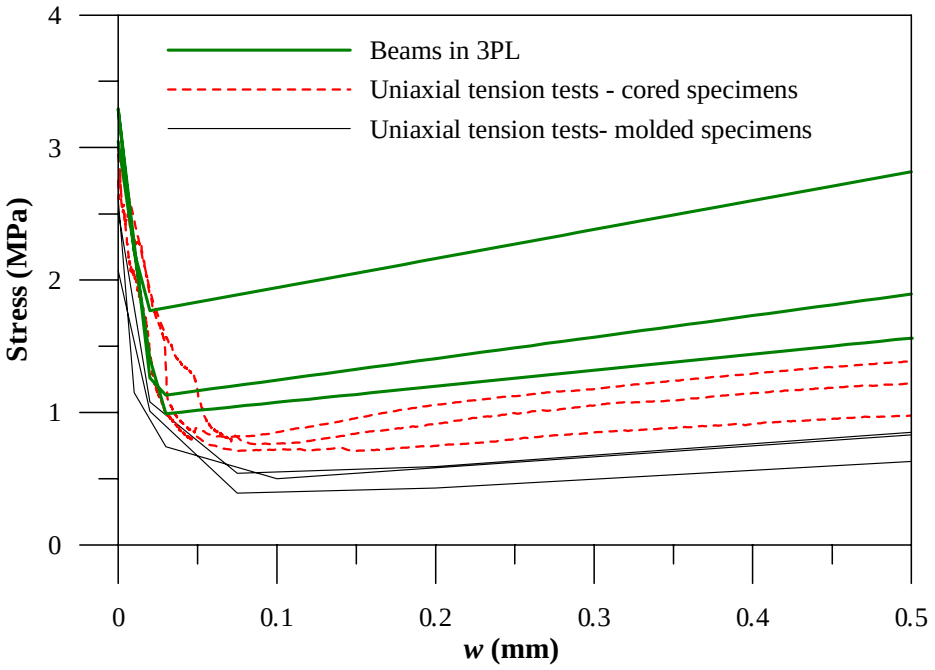

Figure 3.30. σ-*w* curves obtained from inverse analysis of beams compared with results from uniaxial tension tests

3.8. SPLITTING TENSION TESTS

Tests were also performed on cylinders in the splitting-tension configuration, as in Carmona et al. (1998). The test setup is shown in Figure 3.31. The specimen is a 100 mm thick disc cut from a 150 mm diameter specimen. The load is applied over a width of 25 mm with cardboard between the specimen and the loading bars. The test was controlled by means of CMOD measured with a clip gauge (±2.5 mm span and 10 mm gauge length) mounted across the center of the specimen on one of the flat faces (see Figure 3.31). Three specimens were tested in each case.

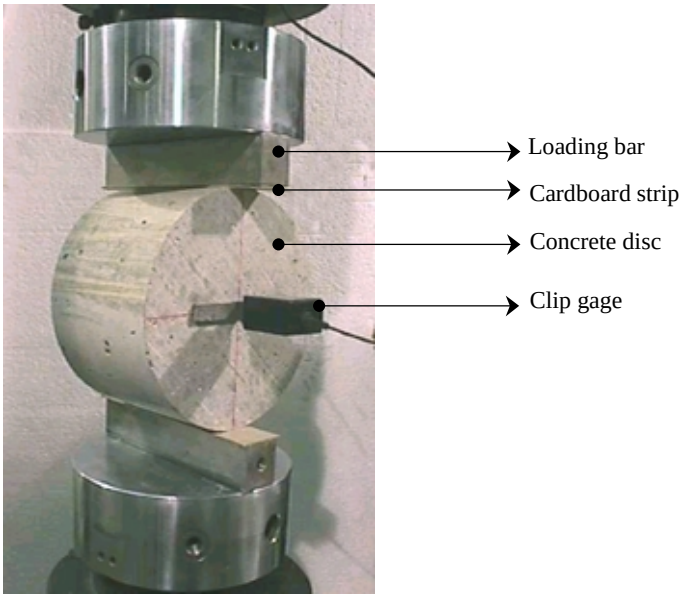

Figure 3.31. Splitting tension test set-up

A typical load-crack opening curve from the splitting-tension test is shown in Figure 3.32, where there is a drop in the load after the peak followed by hardening-type response and a plateau. The load (P) can be used to obtain a nominal tensile stress $\sigma = 2P/\pi dt$, where d and t are the diameter and thickness of the disc. The plot of σ versus the displacement (δ) obtained from the extensometer is given in Figure 3.33a. For comparison, a typical uniaxial tension response from the reference specimen (150×150 mm cylinders) is given alongside in Figure 3.33b. Individual test results are given in Annex B (Figures and Table B.12).

The mean value of the peak stress in the splitting-tension test is 3.0 MPa, which is about 15% higher than the uniaxial tensile strength obtained in the reference test. This relation is accordance with the design equations of Eurocode 2 (1992). The post-peak behavior is, however, significantly different. While the drop in load in the uniaxial tensile test is considerable due to the complete loss of the matrix strength, it appears that in the splitting-tension test, the halves of the specimen continue to carry some of the compressive load. This effect is further aided by the fibers that tie the crack faces leading to hardening-type behavior.

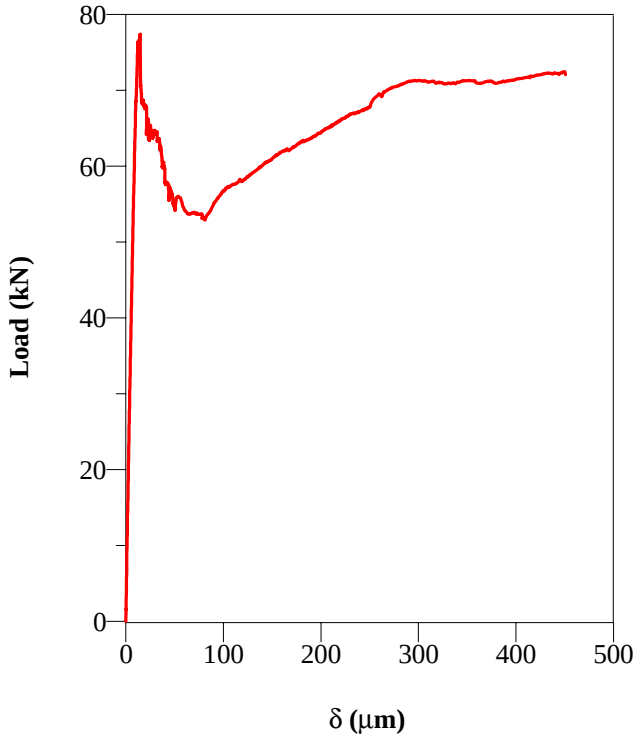

Figure 3.32. Typical load-δ curve from the splitting-tension test

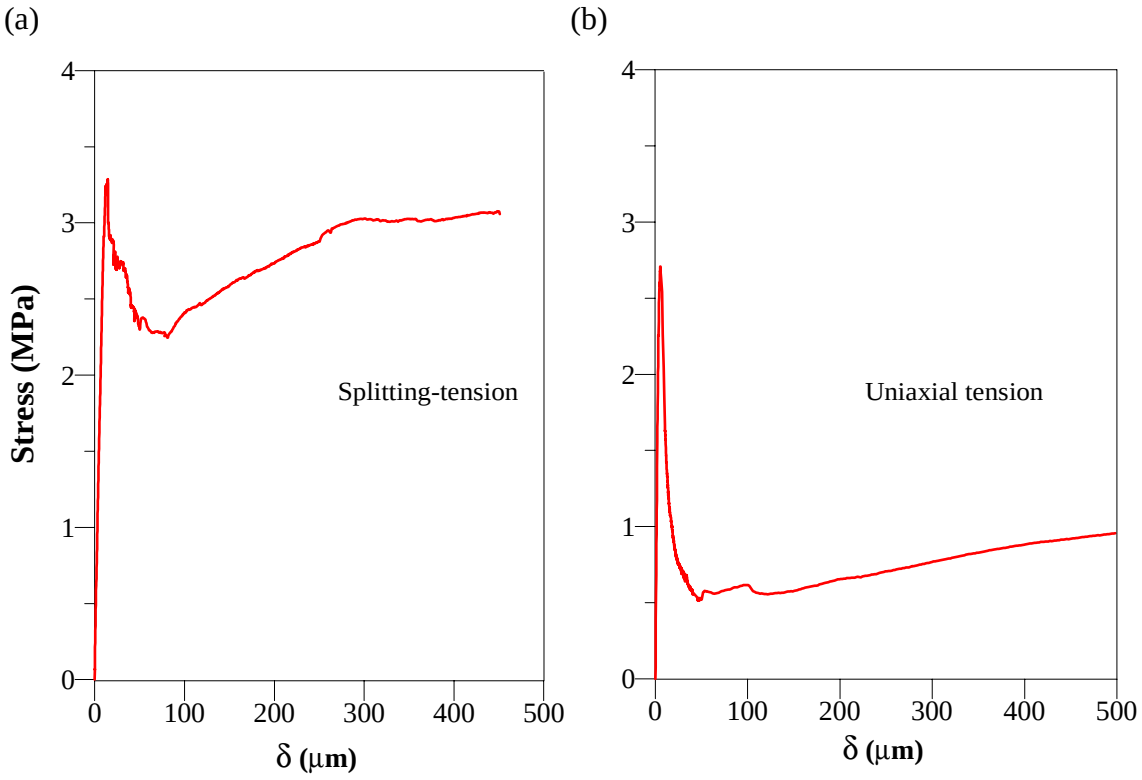

Figure 3.33. Typical σ-δ curves from the (a) splitting-tension and (b) uniaxial tensile tests

3.9. CONCLUSIONS

The study demonstrates that for the analyzed ranges of slenderness and notch depths on cylinders, the uniaxial tensile test of the molded cylinder is robust and valid, with no significant influence of any of the geometrical parameters or problems of instability due to the loss of control in the test. There is some relative rotation between the crack faces until the initial part of the post-peak response, which is attributed to the non-symmetric crack propagation in the matrix. In most of the cases, the rotation decreases in the later part of the post-peak regime.

The stress-crack opening curve can be represented in terms of 4 points using a trilinear form, defined in terms of the stresses determined in the test. This may be more convenient than using the exact curve in finite element or similar analysis.

Effect of fiber orientation on the tensile response has been studied using cores, and is shown that it is important to consider such an effect when vibration is used for compacting the SFRC element. This has also been confirmed by the inverse analysis results from beam tests.

Toughness measures based on the post-peak response can be defined to characterize the behavior of the SFRC or for code-type design methods. Among those considered, the equivalent tensile stress up to a certain crack width seems to be a promising concept, which is readily applicable to constitutive relations of the drop-linear type.

Panels extracted/cut from existing elements for obtaining the stress-crack width relation are not useful since the limited thickness reduces the effectiveness of the fibers and leads to high scatter.

In terms of recommending a 'standard' specimen for further uniaxial tensile testing, a 150 mm long cylinder cut from the middle of a standard 150×300 mm molded cylinder (compacted by tamping to avoid fiber orientation) and having a 15 mm deep circumferential notch at mid-height seems to be optimum. Regarding the measurement of

the displacement, δ, when a stiff test set up is used it is sufficient to measure only the average δ signal from three displacement sensors placed at 120° to each other around the specimen and across the notch.